Analysis, Design and Maximum Power Efficiency Tracking for Undersea Wireless Power Transfer

Taofeek Orekan, *Member, IEEE,* Peng Zhang, *Senior Member, IEEE,* and Cyuansi Shih

***Abstract*—In this paper, a detailed analysis that yields in-depth insight into the design of undersea wireless power transfer system is presented. Based on the analytical results, a methodology for optimized coil design to increase the power transfer efficiency is presented. Owing to the constant motion experienced by undersea wireless power transfer system, a necessary feature is the ability to operate at a multitude of distances without the need for manual tuning to maintain high efficiency. To address this, we propose a novel Maximum Power Efficiency Tracking (MPET) method that uses k-Nearest Neighbors (kNN) to estimate the system's coupling coefficient and tracks the peak efficiency $(> 85\%)$ through an adaptive converter control. Simulation and experimental test results validate the effectiveness and robustness of MPET in achieving maximum wireless power transfer efficiency under a dynamic and uncertain undersea environment.**

***Index Terms*—Maximum power efficiency tracking (MPET), undersea wireless power transfer, k-nearest neighbor, DC-DC converter, smart ocean system.**

I. Introduction

Wireless power transfer (WPT) has been revitalized largely because of the fast expanding market of mobile devices and electric vehicles [1], [2], [3], [4]. Recently, WPT is found to be critically needed in distributed ocean systems that consume excessive power [5], such as an autonomous underwater vehicle (AUV), underwater sensing nodes, ocean monitoring devices, etc. The traditional way of recharging/replacing these devices manually is time-consuming, resulting in limited operation range and disrupted services.

One potential solution is to build underwater docking station with electrical connectors [6], [7], [8], which, however, suffers from high maintenance costs and limits to near shore applications. Here, WPT is investigated as a potent solution to recharge distributed ocean systems. A design concept of WPT for ocean systems application is shown in Fig. 1. The ongoing research of WPT systems is mainly focused on land-based applications [9]. Frequency tuning that automatically adjusts the operating frequency to maximize system efficiency has been developed in [10], [11], [12], [13]. Other methods such as impedance matching [14], [15], [16], intermediate field repeaters [17] [18], and the use of meta-materials [19], [20] to achieve higher power transfer efficiency for WPT in air have also been investigated. Nevertheless, transferring power wirelessly in a marine environment, where seawater is a conducting medium, is still an open and challenging problem.

T. Orekan, P. Zhang are with the Department of Electrical and Computer Engineering, University of Connecticut, Storrs, CT 06269, USA (e-mail: peng.zhang@uconn.edu, taofeek.orekan@uconn.edu)

C. Shih is with the Department of Mechanical Engineering, University of Connecticut, Storrs, CT 06269, USA.

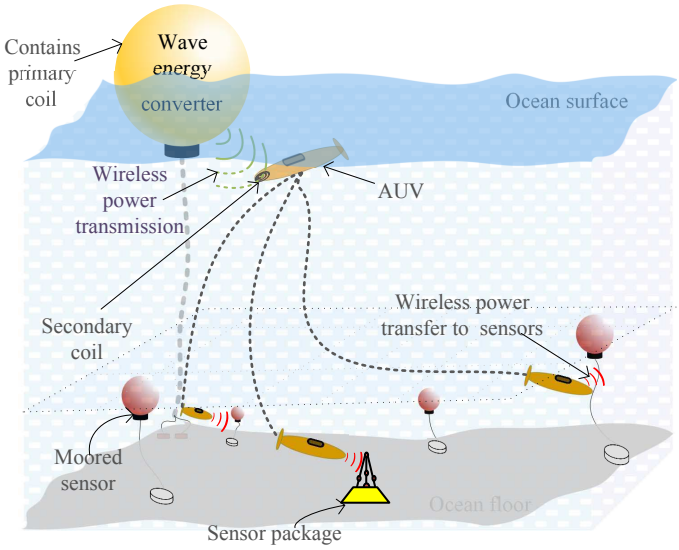

Fig. 1. A design concept of wireless power transfer for ocean systems application.

Several questions to be addressed are: What is the effect of the highly conductive seawater on a WPT system's electrical parameters? What is the effect of seawater on its coil radiation resistance and the losses incurred? If the losses are highly frequency-dependent, then how to choose an operating frequency range in which high efficiency power transfer is possible? Besides, the dynamic nature of the ocean makes the WPT system constantly in motion and leads to time-varying coupling coefficient, which necessitates an optimized design strategy to overcome such expected variability. Furthermore, control methods used in the WPT system in air, such as impedance matching [14], [16], require information from the transmitter through communication to keep track of changes in the system parameters, making them inviable for an undersea WPT (UWPT) system. Rather, a control method that uses information from only the transmitting or receiving side of the system without a communication network is essential.

To address the above challenges, this paper presents a comprehensive UWPT efficiency analysis and MPET control for maximizing undersea power transfer efficiency in real-time. The major contributions of this paper are three-fold.

1) The electrical properties of the UWPT coils submerged in seawater are quantified. The frequency-dependent characteristics of the coil impedance, the self-inductances, mutual inductance, the effects of coil shapes are analyzed and compared to those of WPT in the air.

2) A methodology for optimized coil design to increase power transfer efficiency is developed based on the above analytical results.
3) A novel Maximum Power Efficiency Tracking (MPET) control method is introduced for achieving a maximum power efficiency without communication or feedback from the transmitting side of the UWPT system. In particular, a k-nearest-neighbors-based machine learning approach is devised for a real-time estimation of the coupling coefficient from the receiving side, and the output voltage is directly controlled using a DC-DC converter to track maximum power transfer efficiency.

The estimated coupling coefficient is compared to reference coupling coefficient, and the robustness of the MPET controller is verified through simulations. Also, this work constitutes an extended version of our conference paper in [5].

II. UWPT System Overview

Fig. 2 depicts the equivalent circuit model of the series-series (SS) inductive UWPT system. An SS topology is adopted in this paper because it allows high power to flow on the receiver side, and it is proven to be more efficient than series-parallel and parallel-series circuit topologies [21], [22]. The circuit model includes the 3D geometry of the coils in a marine environment. In the primary side of the system is a transmitter coil (Tx) and in the secondary side is the receiver coil (Rx), which are magnetically coupled by a coupling coefficient $k_{p/s}$. Here L_p, L_s, C_p, C_s, R_p, and R_s represent inductances, series-resonance capacitors, and internal resistances of the primary and secondary circuit, respectively, and the primary and secondary side voltages are defined as V_p and V_s, respectively. The load resistance is R_L. The secondary voltage to primary voltage ratio is derived as:

$$\frac{V_s}{V_p} = \frac{(\omega_0 L_m) R_L}{(R_L + R_s)(R_p R_s + (\omega_0 L_m)^2)} \tag{1}$$

Assuming the transmitting frequency is the same as the resonance frequency of the UWPT, the power transmitting efficiency (η_{pt}) can be written as:

$$\eta_{pt} = \frac{(\omega_0 L_m)^2 R_L}{(R_L + R_s)(R_L R_p + R_p R_s + (\omega_0 L_m)^2)} \tag{2}$$

where

$$\omega_0 = \frac{1}{\sqrt{L_p C_p}} = \frac{1}{\sqrt{L_s C_s}} \tag{3}$$

corresponds to the resonance frequency, and L_m is the mutual inductance which is directly related to the distance between the coils. L_m is responsible for how much power is transferred and its normalized form, coupling coefficient $k_{p/s}$ (defined below), is used to indicate whether the UWPT is over-coupled, critically coupled or under-coupled.

$$k_{p/s} = \frac{L_m}{\sqrt{L_p L_s}}, \qquad 0 \le k_{p/s} \le 1 \tag{4}$$

The undersea environment will modify the electrical characteristics of the UWPT system, which will deteriorate the efficiency of the system. Thus, a critical question is how to optimize the coil design to improve efficiency? The following section is to answer the question.

III. Coil analysis in Underwater Environment

In this section, we aim to understand the essential UWPT parameters, such as the coils' resistance, self-inductance, mutual inductance and resonance frequency, which is critical for optimized coil design and control purposes.

A. Resistance of a coil in seawater

The total resistance of a coil in air or seawater is the sum of the coil's DC resistance (R_{dc}) which depends on the conductor size, the AC resistance (R_{ac}) which is due to its skin depth, and the radiation resistance (R_{rad}). Since the values of R_{dc} and R_{ac} depends on the coil configuration and the quality factor of the wire, they remain almost the same either in seawater or air. However, owing to the conductive nature of seawater ($\sigma_{seawater} \approx 4S/m$), electric currents are induced by the magnetic field surrounding the coils. Hence R_{rad} could differ significantly in seawater than in air [23], [24]. Here, we examine the coil immersed in the seawater and compare it to that in the air through the following formulas [25], [26]:

$$R_{rad}^{sea} = \omega\mu a[\frac{4}{3}(\beta a)^2) - \frac{\pi}{3}(\beta a)^3) + \frac{2\pi}{15}(\beta a)^5) - ...] \tag{5}$$

$$R_{rad}^{air} = \frac{\pi}{6}\frac{\omega^4 \mu a^4}{c^3} \tag{6}$$

where ω is the frequency in radians, μ is the permeability of medium, a is the radius of the coil loop in meters, $\beta{=}(\mu\omega\sigma/2)^{1/2}$, and σ is the conductivity of the medium. As can be seen Fig. 3:

- R_{rad} of the coil in the air is minuscule or almost negligible;
- R_{rad} increases exponentially when the frequency is greater than 200 kHz in seawater.

This means a UWPT transmitter coil should operate under some threshold (e.g., 200 kHz). Otherwise, seawater begins to have a detrimental effect and lead to more losses.

B. Inductance of a coil in seawater

The self-inductance (the ability of a device or component to store energy in the form of a magnetic field) of a circular coil can be calculated using (3). When the transmitter and receiver coils are in close proximity, the current flowing through one of these devices induced a voltage onto the other. This ability to transfer energy inductively is measured by the mutual inductance [27], [28], as expressed below:

$$L_m = \frac{\mu_0}{4\pi} N_p N_s \oiint \frac{e^{-\gamma|R_s - R_p|}}{|R_s - R_p|} dl_p \cdot dl_s \tag{7}$$

where $\gamma \approx \sqrt{j\omega\mu_0\sigma}$, N_p and N_s are the number of turns of the primary and secondary coil, and the circular integrals are over the path of a single turn of each coil. Equation (7) applies to most coil structures except when the coil has very few number of turns and the pitch is very large relative to the wire diameter. Fig. 4 shows the magetic flux variation and the influence of seawater on the characteristics of the mutual inductance between the coils. Actually, the magnetic linkages coupling the coils are significantly reduced as the distance

This article has been accepted for publication in a future issue of this journal, but has not been fully edited. Content may change prior to final publication. Citation information: DOI 10.1109/JESTPE.2017.2735964, IEEE Journal of Emerging and Selected Topics in Power Electronics

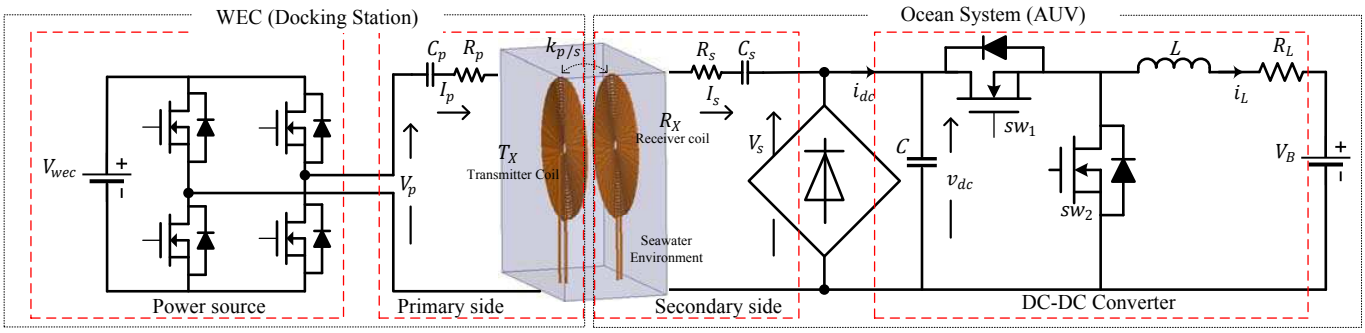

Fig. 2. UWPT system configuration.

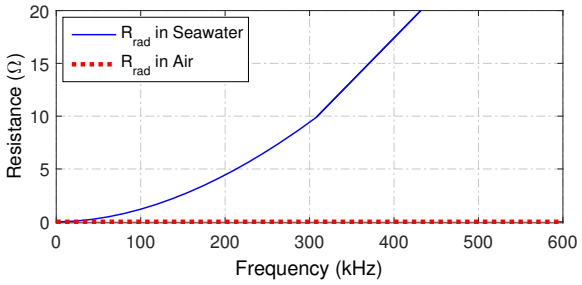

Fig. 3. Simulation result showing comparison between radiation resistance in seawater and air (coil radius=10cm, number of turns=20, wire radius=0.4mm)

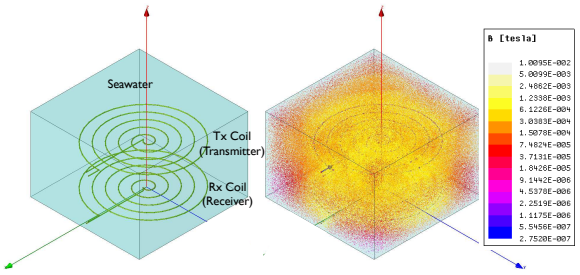

Fig. 4. Magnetic flux distribution in UWPT coil structure in seawater

between Tx and Rx increases, resulting in fast dropping mutual inductance (see Fig. 5c).

Simulation results have been obtained on the UWPT system with spiral-type coils, as shown in Figs. 5a–5d. It can be seen:

- The values of self-inductance of Tx and Rx and the mutual inductance slightly increase as the radius of their coil wires increases from 0.4 to 1-mm (see Figs. 5a–5c)
- The Rx self-inductance varies with distances between Tx and Rx while the Tx self-inductance remains constant (see Figs. 5a and 5b). Given identical Tx and Rx coil radii, the peak value of the self-inductance of Rx can become higher than that of Tx, resulting in compromised power transfer efficiency (see Fig. 5d). The variation in Rx coil is observed to be attributed to the rapid change in distance when the coil is moved away from the Tx coil, in a highly conductive salt water environment. We suspect that the during this change the Rx coil behaves as if it had a solid conductive core to some degree. However, it can be noticed in Fig. 5b that the Rx inductance increase is relatively small and begins to return to its original value as the distance approaches 6 cm.

Consequently, to achieve maximum power transfer, the Tx and Rx coil parameters cannot be identical. Rather, the radius of Rx coil should be made smaller than that of Tx.

C. Coil Topology

It is interesting to determine a UWPT coil topology best suited for integrating ocean distribution system (e.g., AUV). In this paper, the characteristics of spiral-type coil (refer to Fig. 4) and helix-type coil [29] in the undersea environment are comparatively investigated. The design parameters such as coil radius, wire diameter, pitch, and the number of turns of both shapes are made identical for a fair comparison of the effect of the coil shapes. Simulation results are illustrated in Figs. 5e–5h. It can be seen:

- Given the change in distance, the coupling coefficient between the helix coils is much lower than that of the spiral coils. Subsequently, the spiral-type coil is significantly superior to helix-type coil in terms of much higher mutual inductance and as a result higher coupling coefficient. A similar study in [30] shows that when the distance between the coil increases, the efficiency of the spiral coil shape is better than that of helix coil. Therefore, helix-type coil topology is hardly feasible for UWPT application (see Figs. 5e and 5g).
- Increasing the number of turns in helix-type and spiral-type coil topologies, surprisingly, does not improve the coupling coefficient in either case. On the contrary, the coupling coefficient decreases when increasing the number of turns of helix-type coil (see Figs. 5g and 5h).

In real-world situation the wire of the UWPT coil can be protected from seawater using materials such as polyurethane potting and encapsulating materials used on hydrophones. These materials are required to resist the marine environment over long periods of immersion. Based on the above analysis of physical and topological characteristics, we can conclude that the following rules should be considered for design and operation of a UWPT:

1) Low frequency viability (operate at low frequencies);
2) Differentiation criterion (avoid identical Tx and Rx);
3) Close surface proximity (optimize coil topology to enhance coupling).

This article has been accepted for publication in a future issue of this journal, but has not been fully edited. Content may change prior to final publication. Citation information: DOI 10.1109/JESTPE.2017.2735964, IEEE Journal of Emerging and Selected Topics in Power Electronics

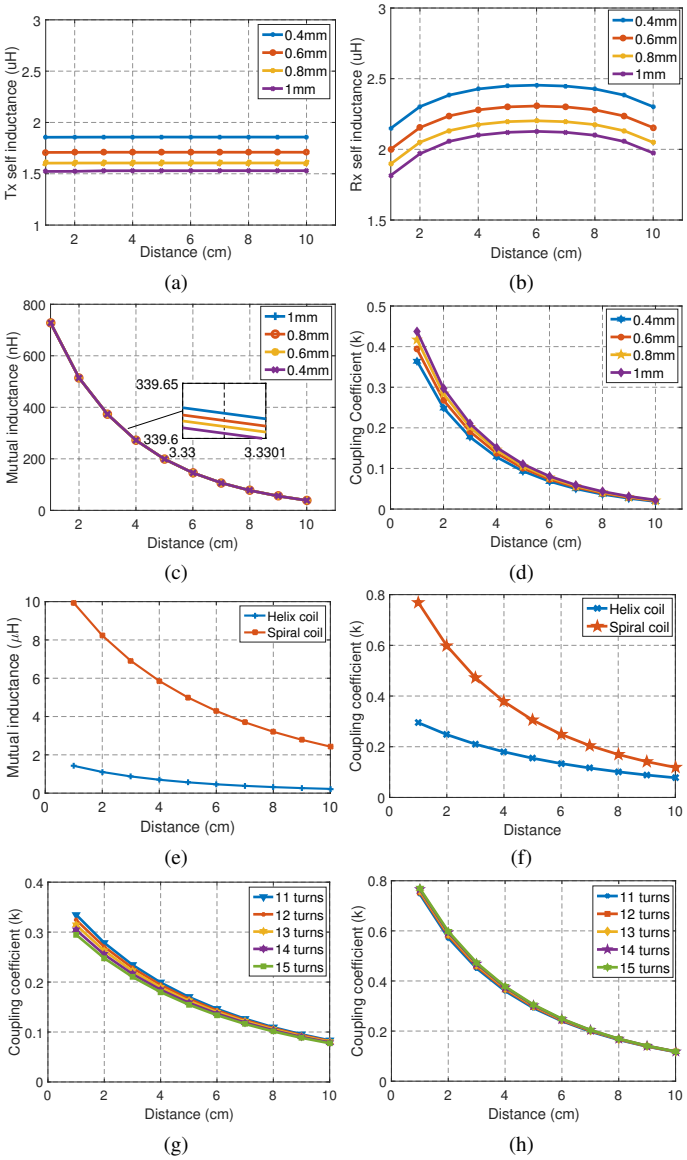

Fig. 5. UWPT coil analysis based on simulation results (Base parameters: Number of turns=20, coil radius=10cm, wire radius=0.4mm; Subplots (a)-(d) obtained on spiral-type coils). (a) Tx self-inductance versus distance at a different wire radius. (b) Rx self inductance versus distance at a different wire radius. (c) Mutual inductance versus distance at a different wire radius. (d) Coupling coefficient versus distance at a different wire radius. (e) Comparison of the mutual inductance between helix and spiral coil shape. (f) Comparison of the coupling coefficient between helix and spiral coil shape. (g) Coupling coefficient versus distance for helix-type coil (h) Coupling coefficient versus distance for spiral-type coil

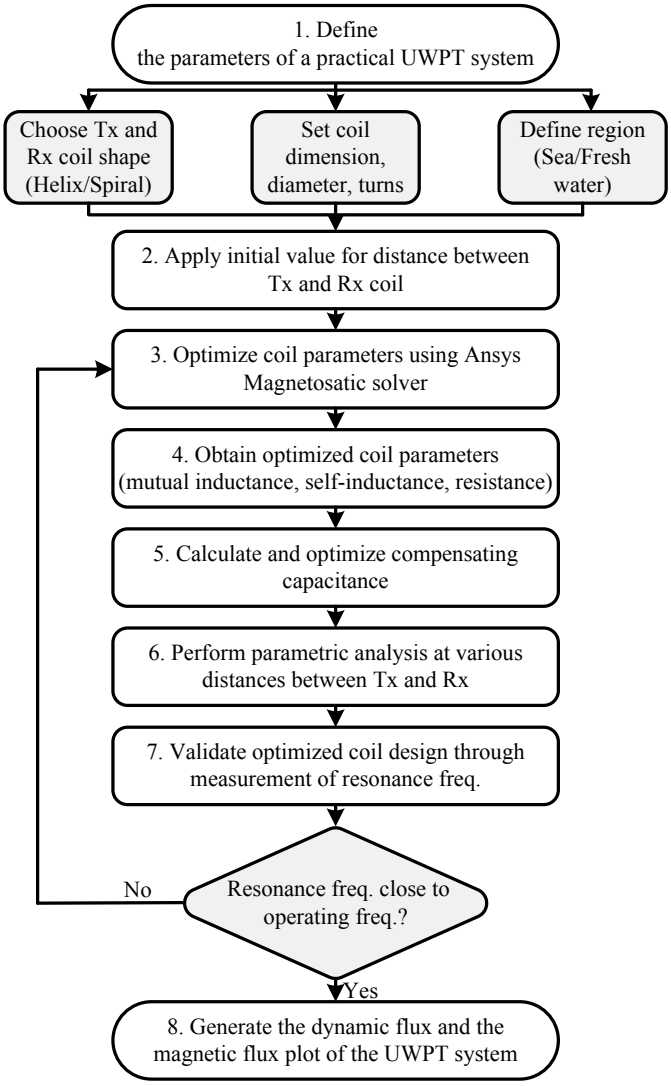

Fig. 6. UWPT optimized coil design flowchart.

IV. Optimized Coil Design Procedure

Enabled by the findings in Section III, we present a systematic method for optimized coil design as depicted in Fig 6. The operating frequency should first be determined according to the power level of the UWPT system and frequency-dependent circuit analysis such as that shown in Fig. 2. The design procedure is presented as follows:

- *Step 1:* The UWPT system design constraints are imposed based on application (e.g., AUV). The coil shape, relative position of windings, the radius of the wire and number of turns are determined, and the 3D model is constructed in finite element (FE) software. A seawater environment is set up, and the associated Maxwell equations are established.
- *Step 2:* Apply the initial value for distance between the transmitter coil Tx and the reciever coil Rx.
- *Step 3:* The coil parameters are computed using a 3D FE magnetostatic solver.
- *Step 4:* The values of self-inductances, mutual inductance and the coupling coefficient between the coils are obtained.
- *Step 5:* Compensating capacitors are chosen based on the resonant frequency and the coil inductances using (3) and (4).
- *Step 6:* Perform parametric sweep on the coils and obtain optimized coil parameters at various distances.
- *Step 7:* Validate optimized coil design through measurement of the resonant frequency using co-simulation with ANSYS Simplorer. Confirm that the optimal frequency is equal or very close to operating frequency.

- *Step 8:* The magnetic fields of the coils calculated based on the optimized parameters of the coil from the magnetostatic analysis.

Since highly precise parameters are needed to get the optimal solution, the above procedure heavily relies on the transient analysis by a FE electromagnetic solver that requires substantial computational resources. Therefore, high-performance computing (HPC) facility is recommended to solve the large-scale simulations with significantly reduced design cycle. For instance, a simulation of a UWPT with 20-turn coil on a PC could take more than 72 hours without guaranteeing to find a solution. Whereas, an 8-core HPC is able to reduce the simulation time to less than 12 hours and achieve faster convergence.

The Table I in Section VI is an instance of an optimized UWPT design using the above procedure.

V. Maximum Power Efficiency Tracking

A. Overview of Maximum Power Efficiency Tracking

The marine environment is highly uncertain and various external forces will cause disturbances on the UWPT system. The coupling coefficient $k_{p/s}$ that determines the power efficiency will fluctuate due to the motion between Tx and Rx (e.g., wave energy converter station and AUV). The purpose of this section is to devise a novel Maximum Power Efficiency Tracking (MPET) that maintains the highest possible power transfer efficiency. For a UWPT deployed in the marine environment the power efficiency is dynamically changing with the load conditions and the coupling coefficient between the coils. There is a need to track the operating point corresponding to the maximum power efficiency. For solar photovoltaic or wind power applications Maximum Power Point Tracking (MPPT) is a well-known concept. For UWPT applications, however, maximum power efficiency is the most important property to be maintained because it is critically important to reduce power losses and preserve energy which is the most scarce resource for undersea applications. Another major difference from traditional MPPT is that our MPET does not need any wireless communication between the transmitter and the receiver which is highly desirable for smart ocean systems. In fact, the k-nearest-neighbors-based machine learning approach is used to estimate the coupling coefficient, making the MPET attractive in practical applications where communication is not viable, such as undersea environment.

First, equation (1) is re-examined to get the secondary voltage:

$$V_s = \frac{(\omega_0 L_m) R_L}{(R_L + R_s)(R_p R_s + (\omega_0 L_m)^2)} V_p \tag{8}$$

V_s changes when the distance between Tx and Rx varies. Fig. 7 depicts the relationship between the V_s and power transfer efficiency at different $k_{p/s}$, under the assumption that the amplitude of the primary voltage V_p and the internal resistance of the primary side coil are constant. As can be seen, to achieve maximum power efficiency at any specific $k_{p/s}$, V_s should be adjusted to an optimal value $V_{s_{max}}$. The reason why $V_{s_{max}}$ (derived below) leads to maximum power efficiency is because

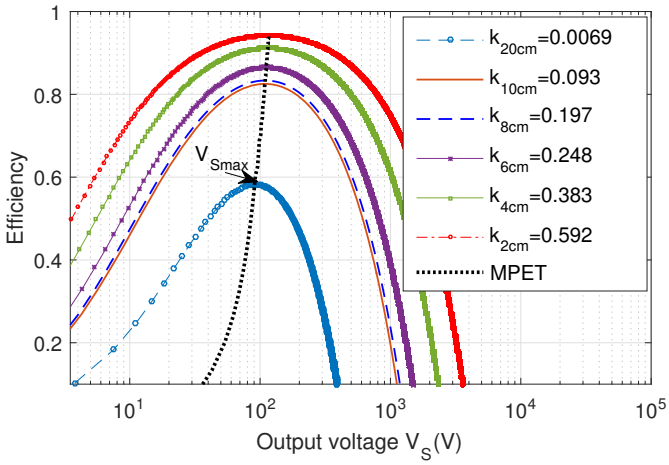

Fig. 7. Output voltage characteristics

$V_{s_{max}}$ correspond to a desirable R_L satisfying the impedance matching condition.

$$V_{s_{max}} = \sqrt{\frac{R_s}{R_p}} \frac{\omega_0 k_{p/s} \sqrt{L_p L_s}}{\sqrt{R_p R_s} + \sqrt{R_p R_s + (\omega_0 k_{p/s})^2 L_p L_s}} V_p \tag{9}$$

Finding $V_{s_{max}}$ becomes a significant challenge as it relies on the real-time information of $k_{p/s}$. One approach is to use in-band wireless communication to transmit information between Tx and Rx, in order to achieve impedance matching. Such approach, however, is no longer viable in a marine environment since fast and cost-effective underwater communication is currently unavailable [31]. To tackle this challenge, we present a novel MPET method to force $V_s \rightarrow V_{s_{max}}$ in real-time using information from the Tx side only without relying on wireless communication.

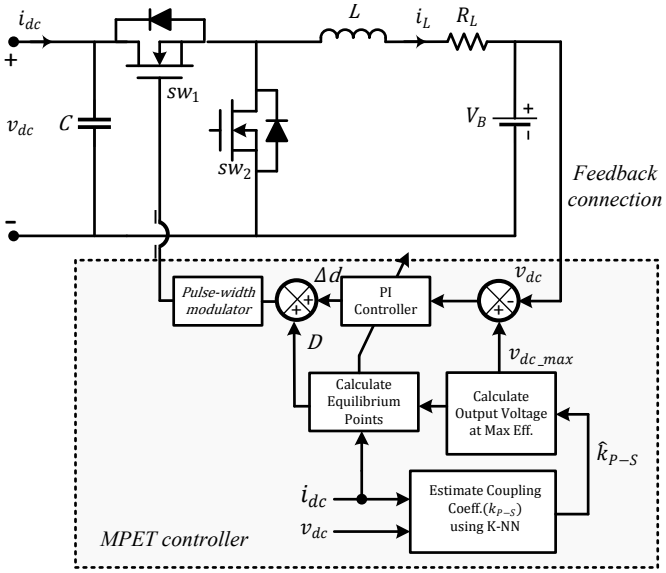

Fig. 8. MPET control block

Fig. 8 summarizes our MPET approach. To be specific, a k-nearest neighbors (kNN) is introduced to estimate $k_{p/s}$

using only Rx information (V_s, I_s). Subsequently, $V_{s_{max}}$ is calculated using (9) and serves as the reference for feedback control to track. As a salient feature, our MPET is an adaptive tracker that updates the PI controller in real-time, and it employs a DC-DC converter to achieve the task of changing output voltage to desire voltage by adjust the duty ratio. This feature makes the UWPT more resilient to the fast changing $k_{p/s}$.

B. Estimation of Coupling Coefficient

The Kirchhoff's voltage law (KVL) equations for the UWPT system in Fig. 2 (Tx and Rx side) can be derived as:

$$\begin{aligned} V_p &= R_p I_p + \omega_0 k_{p/s} I_p \sqrt{L_p L_s} \\ V_s &= \omega_0 k_{p/s} \sqrt{L_p L_s} I_s + R_s I_s \end{aligned} \tag{10}$$

Thus $k_{p/s}$ can be estimated by

$$\hat{k}_{p/s} = \frac{V_p \pm \sqrt{V_p^2 - 4R_p I_s (V_s + R_p I_s)}}{2 I_s \omega_0 \sqrt{L_p L_s}} \tag{11}$$

$\hat{k}_{p/s}$ is subject to uncertainties on the Tx and Rx sides. Furthermore, it is infeasible to track both Tx and Rx states in real-time without communication. To tackle the challenges, we proposed a data-driven approach, kNN, for robust estimation of $\hat{k}_{p/s}$ under uncertainties, through local approximation using recursive procedure. In particular, $\hat{k}_{p/s}$ is learned from the secondary voltages and currents as shown in algorithm 1.

Algorithm 1 Coupling coefficient estimation

1: Generate the dataset of pairs:
$(x_1, y_1), (x_2, y_2), ..., (x_N, y_N)$ where,
$y_i = V_p + \sqrt{V_p^2 - 4R_p I_s (V_{s,i} + R_s I_{s,i})}$
$x_i = 2 I_{s,i}\, \omega_0 \sqrt{L_p L_s}$
2: Set a query point: x_q
3: Compute the Euclidean distance from the query point to the labeled dataset using
$distance(x_i, x_q) = \sqrt{a_1 (x_i - x_q)^2 + \cdots + a_n (x_n - x_q)^2}$
4: Sort the labeled samples in ascending order of distance
5: Find k closest x_i in dataset $(x_{NN1}, ...x_{NNk})$ such that for any x_i not in nearest neighbor set $distance(x_i, x_q) \geq distance(x_{NNK}, x_q)$
6: Find a heuristic number k of nearest neighbors
7: Estimate the coupling coefficient which $k_{p/s}$ using knearest neighbors $\overline{y} = \frac{1}{k}(y_{NN1} + \cdots + y_{NNK})$

Note that the real parts of the dominating poles in the transfer functions from the primary and secondary voltages to the secondary current are much faster than the fluctuation frequency of coupling coefficient [32]. This means that the transient response attenuate quickly and will hold true under dynamics environment. Thus $k_{p/s}$ remains static in the UWPT. This guarantees the validity and robustness of the proposed kNN estimation method.

C. Modeling of the DC-DC converter

When reaching steady state, the DC-DC converter in Fig. 8 can be represented by an average state-space model as follows:

$$\begin{aligned} 0 &= \mathbf{A}_{av} X + \mathbf{B}_{av} U \\ V_{dc} &= \mathbf{C}_{av} X \end{aligned} \tag{12}$$

where

$$\mathbf{A}_{av} = \begin{bmatrix} 0 & -\frac{D}{C} \\ \frac{D}{L} & -\frac{R_b}{L} \end{bmatrix}, \mathbf{B}_{av} = \begin{bmatrix} \frac{1}{C} & 0 \\ 0 & -\frac{1}{L} \end{bmatrix}, \mathbf{C}_{av} = \begin{bmatrix} 1 & 0 \end{bmatrix}$$
$$X = \begin{bmatrix} V_{dc} \\ I_L \end{bmatrix}, U = \begin{bmatrix} I_{dc} \\ V_b \end{bmatrix}$$

L, R_b, v_{dc} and C are the inductance, the battery resistance, the DC-link voltage, and the filter capacitor, respectively. The battery voltage is V_b and the current flowing into the battery is I_L. The DC-DC converter states can then be found, as follows:

$$I_L = \frac{I_{dc}}{D} \tag{13}$$

$$V_{dc} = \frac{V_b D + I_{dc} R_b}{D^2} \tag{14}$$

where

$$D = \frac{V_B \pm \sqrt{{V_B}^2 + 4 V_{dc} I_{dc} R_B}}{2 V_{dc}} \tag{15}$$

I_{dc}, I_L, V_{dc}, and D are the steady-state values of $i_{dc}(t)$, i_L(t), $v_{dc}(t)$, and Δd, respectively.

During transient-state, to maintain a desired level of performance of the MPET, discussed in the next section is a PI controller that adjusts the error caused by the difference between the output voltage V_{dc} and the reference voltage $V_{dc_{max}}$, toward its original steady state values.

D. Controller Design

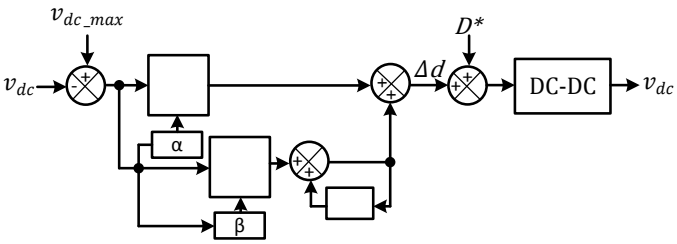

Fig. 9. PI Controller Design

The control objective here is to adjust the output voltage of the DC-DC buck converter towards the designated output voltage on the load side, under all possible operating conditions. The output voltage of DC-DC converter is a function of the duty cycle Δd. In order to regulated the output voltage, the DC-DC converter should be controlled to regulate its duty cycle.

We introduce an adaptive PI controller (see Fig. 9) that adjust PI parameters in real-time [33]. This method is preferable in that it achieves a desired level of performance of the MPET control system when Δd change with time. The proportional constant (K_P) and integral constant (K_I) of the

This article has been accepted for publication in a future issue of this journal, but has not been fully edited. Content may change prior to final publication. Citation information: DOI 10.1109/JESTPE.2017.2735964, IEEE Journal of Emerging and Selected Topics in Power Electronics

TABLE I
UWPT SYSTEM PARAMETERS

Parameters	Tx side	Rx side
Coil radius (cm)	6	5
Number of turns	20	18
Wire diameter (mm)	0.6	1
Self-inductance (μH)	47 .8	20.3
Parasitic resistance (ohms)	1.3	1.3
Capacitor (nF)	53.1	38.5
Operating frequency (kHz)	178	178
AC voltage source (V)	150	–
Switching frequency (KHz)	–	100
Load resistance (Ω)	–	50

PI are adaptively adjusted by adjusting the values of α and β, respectively. The transfer function of the PI controller is described as follows:

$$G_{PI}(s) = K_P + \frac{K_I}{s} \tag{16}$$

α and β (whose values are K_P and K_I respectively during the steady state) are adaptively varied as a function of error signal v_{err} value, so as to drive the steady state error to zero. As a result, the dynamic output voltage deviation and the settling time of the output voltage are reduced.

VI. Simulation Results

The effectiveness of MPET has been verified on a UWPT system with a primary voltage V_p of 150 V, an coil operating frequency of 178 kHz and a switching frequency of 100 kHz in its DC-DC converter. Three test cases are performed by using MATLAB/Simulink and ANSYS Maxwell & Simplorer. The first test case is to examine the resonant frequency at which high power transfer efficiency of UWPT is expected. The second test case is to validate the performance of kNN-based coupling coefficient estimation. The third test case is to verify the proposed MPET approach. The optimized UWPT parameters used in the case studies are listed in Table I.

A. UWPT Resonance Frequency Analysis

To figure out the resonant frequency, the load of UWPT system is varied from 10 Ω to 100 Ω with a step of 10 Ω while the distance between Tx and Rx coils is fixed at 1 cm (i.e., $k_{p/s}$ fixed at 0.18).

As shown in Fig. 10, there exists an optimal resonance frequency (i.e., 178 kHz) where a maximum efficiency is consistently achieved even though the load varies between 10 Ω and 100 Ω. Therefore, the test UWPT system is to be operated at 178 kHz in the following tests. It should be pointed out, however, that the power transfer efficiency will vary significantly as coupling coefficient between the transmitter coil and the receiver coil varies (see Fig. 11). This means that both the on-line coupling coefficient estimation and MPET are indispensable to maintain high UWPT efficiency in the ever-changing marine environment.

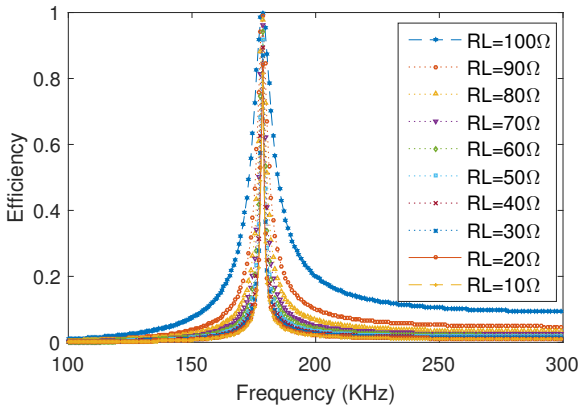

Fig. 10. UWPT system efficiency (at $k_{P/S} = 0.18$) as a function of frequency. Target resonance frequency set at 178 kHz for a wide range of load resistance.

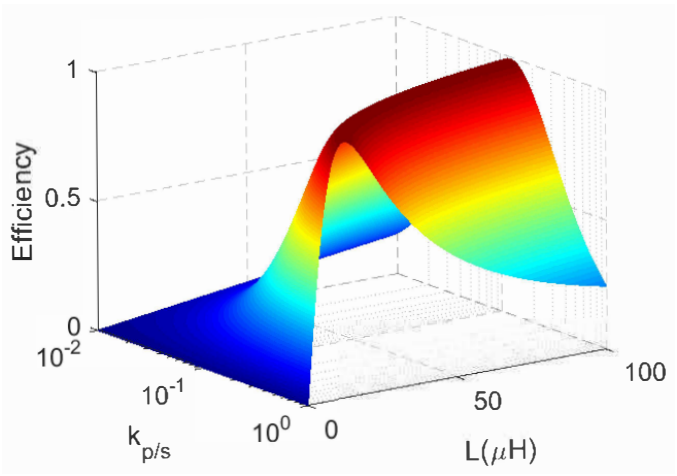

(a)

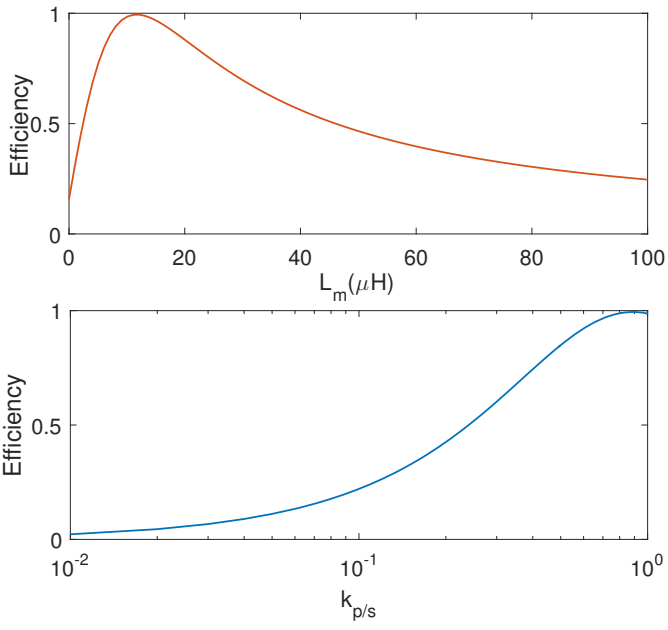

(b)

Fig. 11. Simulation result showing the relationship between the coupling coefficient $k_{p/s}$, mutual inductance L_m, and efficiency at the same resonant frequency $f_0 = 178kHz$.

This article has been accepted for publication in a future issue of this journal, but has not been fully edited. Content may change prior to final publication. Citation information: DOI 10.1109/JESTPE.2017.2735964, IEEE Journal of Emerging and Selected Topics in Power Electronics

B. Coupling Coefficient Estimation

This case performs the kNN-based on-line estimation of the coupling coefficient. For verification purpose, the exact values of $k_{p/s}$ between the transmitter coil and the receiver coil are analytically obtained from the simulated dataset of primary and secondary circuit parameters. The kNN-based on-line estimation is then performed under a specific condition (e.g., a resonant frequency of 178 kHz and a load impedance of 50 Ω). The comparison between the estimated $\hat{k}_{p/s}$ values and the exact values demonstrates the accuracy and efficiency of the proposed estimation approach (see Fig12). In fact, it takes less than 6.123s CPU time to obtain 1000 estimated $\hat{k}_{p/s}$ values with a maximum error of around 5%. It can be seen that the maximum error occurs due to radiation loss when the distance between Tx and Rx increases. This error can be reduced by sampling more data at a longer period and filtering measurement error. This proves the kNN-based approach is well suited for the real-time MPET. More estimation results under different loading conditions have been obtained by using impedance sweep, which have consistently verified the accuracy and effectiveness of the kNN-based estimation approach. Those results are omitted due to the space limit.

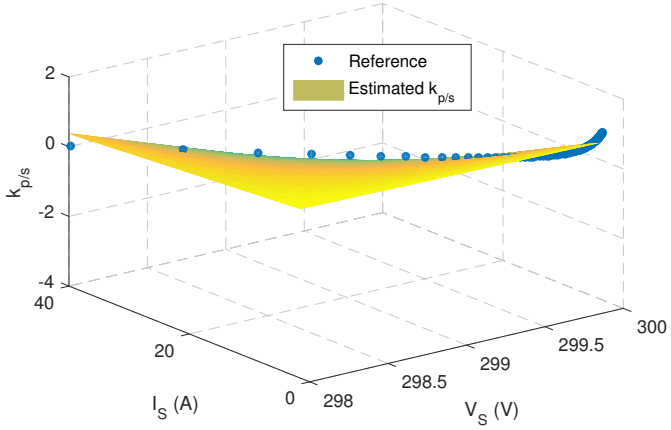

(a)

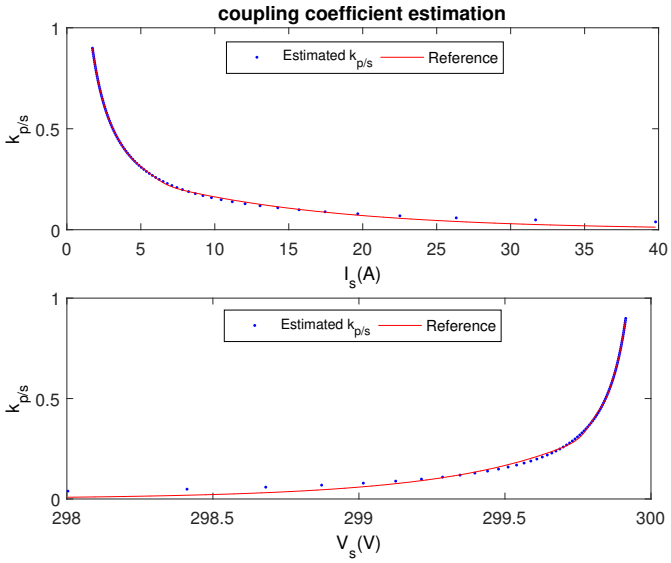

(b)

Fig. 12. Simulation result showing the comparison between reference coupling coefficient (kp/s) and estimated coupling coefficient ($\hat{k_{p/s}}$) (a) Coupling coefficient estimation in 3D (b) Coupling coefficient estimation in 2D

C. UWPT Efficiency Maximization

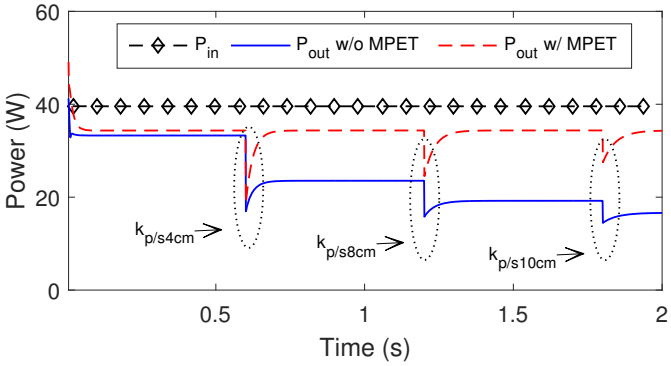

(a)

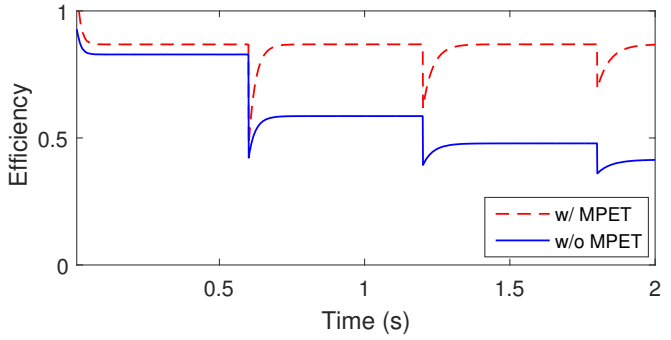

(b)

Fig. 13. Simulation result of MPET control for UWPT system. (a) UWPT power output with and without MPET control (b) Maximum efficiency with and without MPET control.

The effectiveness of MPET is extensively evaluated on a dynamic UWPT model subject to fast position changes, by using ANSYS Maxwell & Simplorer and MATLAB/Simulink. The former is employed to perform the transient analysis of the UWPT, in order to obtain the values of the optimized coil parameters. The latter run simulations with the Tustin solver at a time-step of 10 μs to verify MPET.

In this test, the transmitter coil is fixed while the receiver coil is originally placed at 1 cm and then quickly moved further away at 4 cm, 8 cm and 10 cm. The output powers and efficiencies of the UWPT system with and without MPET are measured and illustrated in Fig.13. With MPET, when the distance increases, a maximum power efficiency of 85% can be consistently tracked and a power transfer of 34W is achieved. Without MPET, however, the output powers decline and the efficiencies decreases drastically from 85% to 39% as the distance increases. It can also be seen that, when the distance between the coils has a step (or near-step) change, MPET is always able to quickly restore the maximum power efficiency within 0.1 s, which validates the effectiveness and robustness of the MPET.

This article has been accepted for publication in a future issue of this journal, but has not been fully edited. Content may change prior to final publication. Citation information: DOI 10.1109/JESTPE.2017.2735964, IEEE Journal of Emerging and Selected Topics in Power Electronics

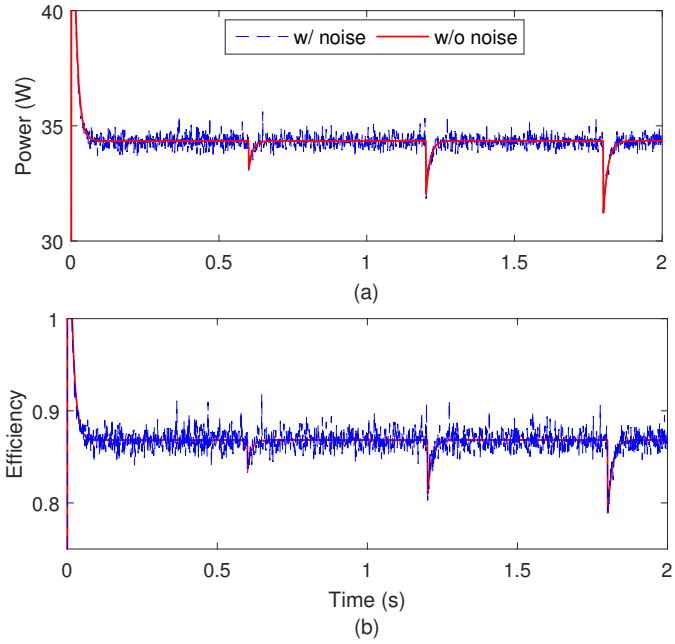

Fig. 14. Simulation result showing the response of MPET when subject to Additive white Gaussian noise (SNR=6db). (a) UWPT power output with and without noise (b) Maximum efficiency with and without noise

To further verify the robustness of MPET, the same test is performed in a noisy environment when the output voltage feedback signal and the PI controller are subject to an additive white Gaussian noise with a signal to noise ratio of 6 db. Fig.14 shows that MPET remains highly efficient and robust under such noisy environment.

VII. Experimental Verification

To verify the analysis above, an experimental UWPT prototype is implemented, as shown in Fig. 15. The experimental setup consists of a power supply, transmitter and receiver coils, micro-controller and power electronics converter, and a digital oscilloscope. The target resonant frequency is set as 178KHz, and the parameters used in this experiment system are set to be the same as those in the simulations, except for the input voltage which is set at 30V due to hardware limitation. All submerged tests for the experiment are implemented in a 20-gallon fish tank filled with seawater of 3.63% salt. Hence, these solutions reasonably models a marine environment. Based on the coil analysis in Section III, the coils are fabricated in a flat spiral disk using 22 AWG wire, and their self-inductances are measured using a complex impedance analyzer. As shown in Fig. 16, the coils are placed onto a 3D printed disks to hold them in place. The input and output cables are connected to the Tx and Rx coil, respectively, and mounted on a test rig that adjusts the distance between the coils.

On the transmitting side of the UWPT system, a DC source is used to provide a constant voltage to an operational power amplifier (APEX PA 94a) at 178KHz generated by a function generator. The function generator used here could be replaced by either a standalone function generator IC, or be created using software on a micro-controller. The DC power supply

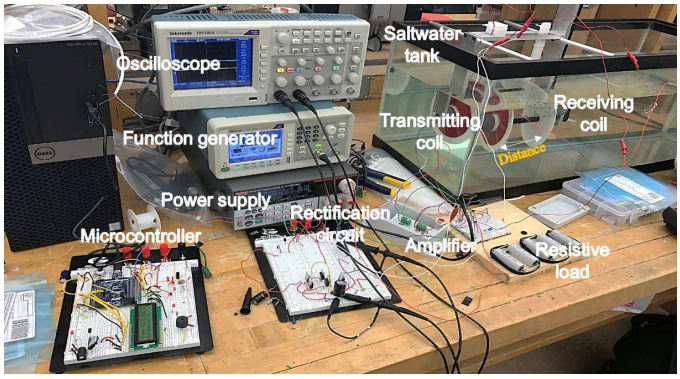

Fig. 15. Experimental setup of UWPT.

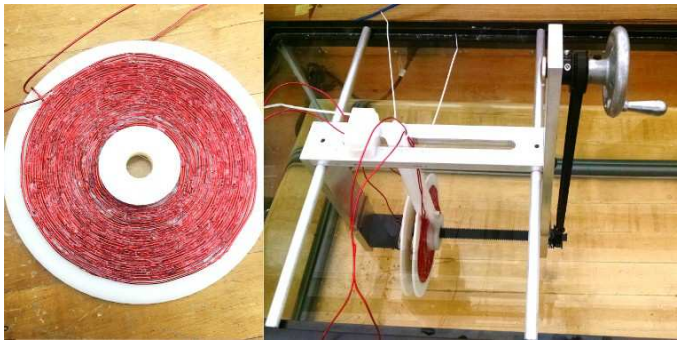

Fig. 16. UWPT transmitter and receiver test coil

of the power amplifier is set to its maximum range $\pm 30V$, creating an AC voltage of 30Vpp across the TX coil.

Meanwhile, on the receiving end of the UWPT system, four SBR10U40CT diodes are used to build a standard full bridge rectifier which converts the transferred AC voltage signal to DC. A DC-DC buck converter described in Section V subsequently used to step-down the voltage to a desired voltage level. The control unit ATmega328p includes a 10-bit analog-to-digital converter, which converter the voltage and current to digitized data used to execute MPET.

Fig. 17 shows the measured results of the UWPT system; when the Rx coil is placed at 1cm, 2cm, 3cm, and 4cm away from the Tx coil. It can be seen that the voltage received by the RX coil gradually reduces as the distance between the transmitter and the receiver increases. Fig 17a -17d corresponds to power transfer efficiencies of 80%, 73%, 66%, and 58%, respectively, through seawater. Fig. 18 gives the measured power efficiency compared against the simulation results, which shows close agreement between simulations and experiments.

Fig. 19a shows the resonant frequency obtained by applying the Fast Fourier Transform (FFT) on the raw data from the oscilloscope. The result shows the power transfer efficiency is maximized at the target resonant frequency. As the distance increases from 1-10cm (target distance range of the UWPT) the efficiency is still greater than 80%. However, when the distance increases beyond the target range, the seawater begins to have detrimental effect on the system and the efficiency quickly decreases below 50% at the resonant frequency of

This article has been accepted for publication in a future issue of this journal, but has not been fully edited. Content may change prior to final publication. Citation information: DOI 10.1109/JESTPE.2017.2735964, IEEE Journal of Emerging and Selected Topics in Power Electronics

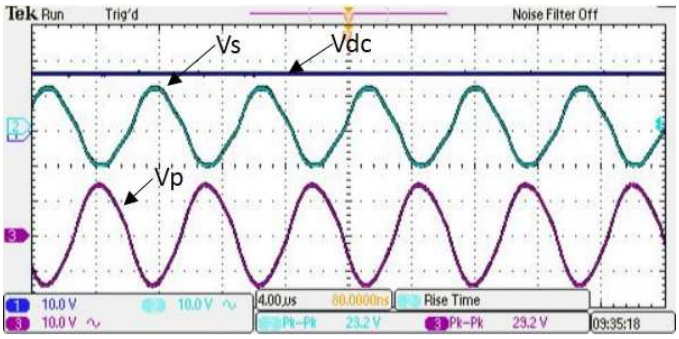

(a)

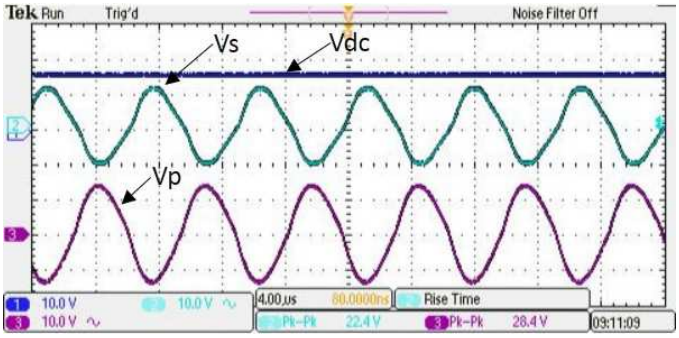

(b)

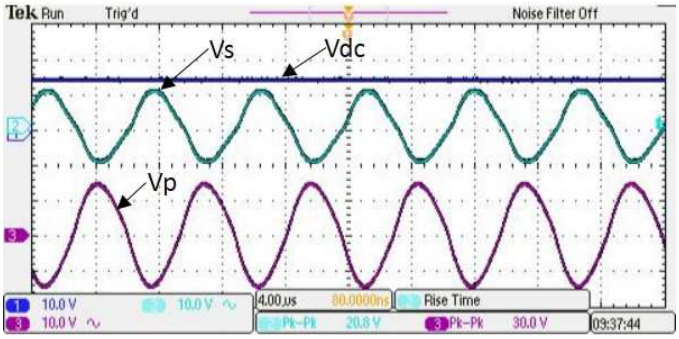

(c)

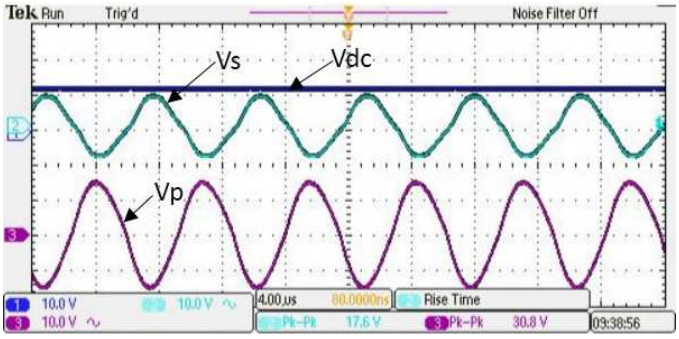

(d)

Fig. 17. Part of the experimental results. Transmitter and receiver voltage waveform (a) at a distance of 1cm (b) at a distance of 2cm (c) at a distance of 3cm (c) and at a distance of 4cm

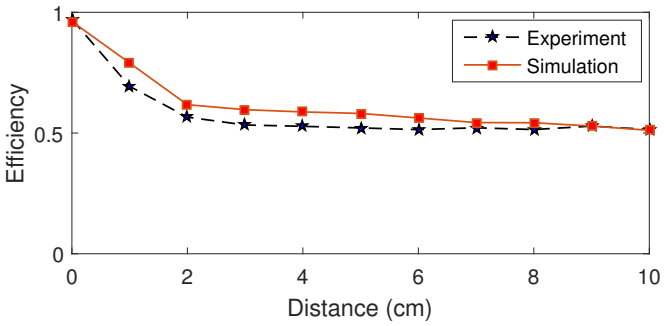

Fig. 18. Measured experimental result of the UWPT power transfer efficiency at a distance between 1-10cm.

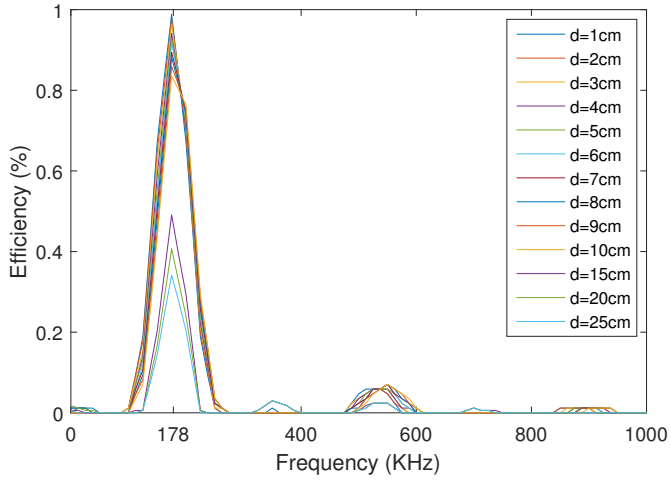

(a)

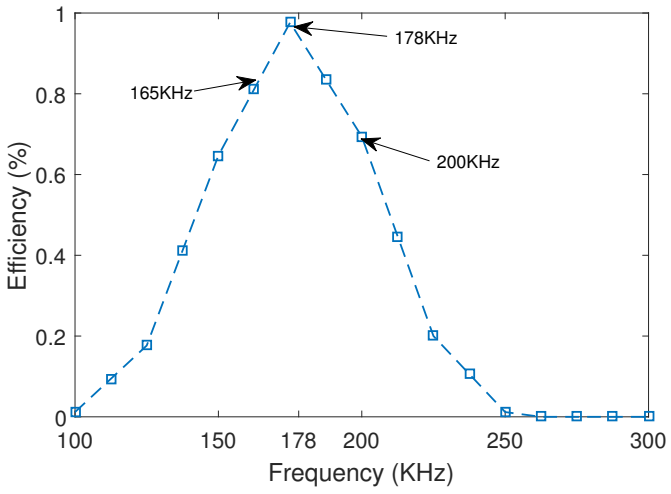

(b)

Fig. 19. Experimental results of UWPT resonance frequency (Target frequency is set at 178KHz). (a) Resonant frequency at a distance between 1-10cm versus efficiency (b) Sensitivity of the resonance frequency

178KHz. Fig. 19b shows the sensitivity of the UWPT system when its deviate from the resonant frequency. Even though a high efficiency of 80% is still feasible when the resonant frequency deviate into a frequency range of [165KHz, 185KHz] a variable capacitor is recommended to be used at the transmitter side to bring the resonant frequency to its precise value as in [34].

In Fig. 20a, when the distance between the Tx coil and the Rx coil increases without control, the output voltage Vdc after rectification drops significantly. In practice, as shown in Fig. 20b, the buck converter can be controlled to regulate the

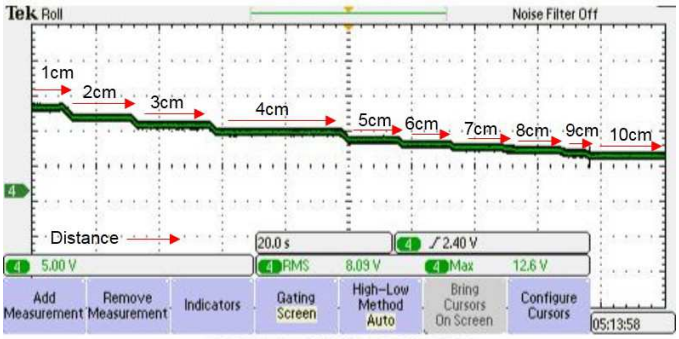

(a)

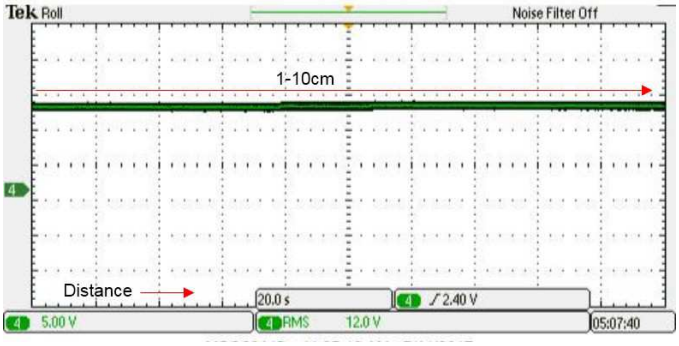

(b)

Fig. 20. Experimental results of the UWPT system. (a) Without control when distance is adjusted from 1-10cm at unfixed interval (b) Controlled to a regulated output voltage of 12V.

output voltage at 12V in spite of the changes of the distance between Tx and Rx.

VIII. Conclusion

This paper provides a deep understanding of transferring power wirelessly in a dynamic undersea environment. Factors that affect power transfer efficiency are analyzed in detail. A systematic design approach is developed to optimize the coil properties and thus improve the overall system efficiency. A novel Maximum Power Efficiency Tracking (MPET) method is then developed to estimate UWPT coupling coefficient in real-time through machine learning and to effectively track the maximum power efficiency ($> 85\%$) when UWPT is subject to the motion of the sea. Extensive simulation and experimental tests have validated the effectiveness of the analysis, design and MPET approaches. The systematic methods in this paper have opened a new door of opportunities for smart ocean systems research. Our future research will be focused on MPET for multiple source ocean energy systems, new power electronic topologies that enables load variation across broader range for better estimation purpose in MPET, as well as advanced control strategies for MPET.

Acknowledgment

This material is based upon work supported by the National Science Foundation under Grant No. 1647209 and Eversource Energy Center under Grant No. 6200980.

The authors gratefully acknowledge the contributions of Prof. Shengli Zhou for his valuable comments and helpful suggestions. The authors would also like to thank Alex Slossberg, Frank Ludorf, Walters Justin, and Kyle Buckley for their assistance in setting up the hardware prototype of the UWPT system.

References

[1] Witricity. [Online]. Available: http://www.witricity.com/
[2] Qualcomm/haloipt. [Online]. Available: http://www.qualcomm.com
[3] J. M. Miller, O. C. Onar, and M. Chinthavali, "Primary-side power flow control of wireless power transfer for electric vehicle charging," *IEEE J. Emerg. Sel. Topics Power Electron.*, vol. 3, no. 1, pp. 147–162, Mar. 2015.
[4] S. Y. R. Hui, W. Zhong, and C. K. Lee, "A critical review of recent progress in mid-range wireless power transfer," *IEEE Trans. Power Electrons.*, vol. 29, no. 9, pp. 4500–4511, Sept. 2014.
[5] T. M. Hayslett, T. Orekan, and P. Zhang, "Underwater wireless power transfer for ocean system applications," in *OCEANS 2016 MTS/IEEE Monterey*, Sept. 2016.
[6] R. S. McEwen, B. W. Hobson, and L. McBride, "Docking control system for a 54-cm-diameter (21-in) auv," *IEEE J. Ocean. Eng.*, vol. 33, no. 4, pp. 550–562, Oct. 2008.
[7] R. Stokey, B. Allen, and T. Austin, "Enabling technologies for remus docking: an integral component of an autonomous ocean-sampling network," *IEEE J. Ocean. Eng.*, vol. 26, no. 4, pp. 487–497, Oct. 2001.
[8] K. Teo, E. An, and P. J. Beaujean, "A robust fuzzy autonomous underwater vehicle (auv) docking approach for unknown current disturbances," *IEEE J. Ocean. Eng.*, vol. 37, no. 2, pp. 143–155, Apr. 2012.
[9] W. Zhong and S. Y. R. Hui, "Maximum energy efficiency tracking for wireless power transfer systems," *IEEE Trans. Power Electrons.*, vol. 30, no. 7, pp. 4025–4034, Jul. 2015.
[10] A. P. Sample, D. Meyer, and J. R. Smith, "Analysis, experimental results, and range adaptation of magnetically coupled resonators for wireless power transfer," *IEEE Trans. Ind. Electron.*, vol. 58, no. 2, pp. 544–554, Feb. 2011.
[11] N. Y. Kim, K. Y. Kim, J. Choi, and C. W. Kim, "Adaptive frequency with power-level tracking system for efficient magnetic resonance wireless power transfer," *Electron. Lett.*, vol. 48, no. 8, pp. 452–454, Apr. 2012.
[12] B. H. Waters, A. P. Sample, P. Bonde, and J. R. Smith, "Powering a ventricular assist device (vad) with the free-range resonant electrical energy delivery (free-d) system," *Proc. IEEE*, vol. 100, no. 1, pp. 138–149, Jan. 2012.
[13] Z. Pantic, K. Lee, and S. M. Lukic, "Receivers for multifrequency wireless power transfer: Design for minimum interference," *IEEE J. Emerg. Sel. Topics Power Electron.*, vol. 3, no. 1, pp. 234–241, Mar. 2015.
[14] J. Park, Y. Tak, Y. Kim, Y. Kim, and S. Nam, "Investigation of adaptive impedance matching methods for near-field wireless power transfer," *IEEE Trans. Antennas Propag.*, vol. 59, no. 5, pp. 1769–1773, May May 2011.
[15] L. Huang, A. P. Hu, A. K. Swain, and Y. Su, "Z-impedance compensation for wireless power transfer based on electric field," *IEEE Trans. Power Electron*, vol. 31, no. 11, pp. 7556–7563, Nov. 2016.
[16] T. C. Beh, T. Imura, M. Kato, and Y. Hori, "Basic study of improving efficiency of wireless power transfer via magnetic resonance coupling based on impedance matching," in *IEEE Int. Symp. Ind. Electron*, 7 Jul. 2010.
[17] F. Zhang, S. A. Hackworth, W. Fu, C. Li, Z. Mao, and M. Sun, "Relay effect of wireless power transfer using strongly coupled magnetic resonances," *IEEE Trans. Magn.*, vol. 47, no. 5, pp. 1478–1481, May May 2011.
[18] D. Ahn and S. Hong, "A study on magnetic field repeater in wireless power transfer," *IEEE Trans. Ind. Electron.*, vol. 60, no. 1, pp. 360–371, Jan. 2013.
[19] M. J. Chabalko, J. Besnoff, and D. S. Ricketts, "Magnetic field enhancement in wireless power with metamaterials and magnetic resonant couplers," *IEEE Antennas Wireless Propag. Lett.*, vol. 15, pp. 452–455, Jul. 2015.
[20] E. S. Rodrguez, A. K. RamRakhyani, and D. Schurig, "Compact low-frequency metamaterial design for wireless power transfer efficiency enhancement," *IEEE Trans. Microw. Theory Tech.*, vol. 64, no. 5, pp. 1644–1654, May 2016.
[21] M. Ishihara, K. Umetani, H. Umegami, E.Hiraki, and M. Yamamoto, "Quasi-duality between ss and sp topologies of basic electric-field coupling wireless power transfer system," *Electron. Lett.*, vol. 52, no. 25, pp. 2057–2059, Dec. 2016.

[22] T. Campi, S. Cruciani, F. Maradei, and M. Feliziani, "Near-field reduction in a wireless power transfer system using lcc compensation," *IEEE Trans. Electromagn. Compat.*, vol. 59, no. 2, pp. 686–694, Apr. 2017.
[23] K. Iizuka, R. King, and C. Harrison, "Self- and mutual admittances of two identical circular loop antennas in a conducting medium and in air," *IEEE Trans. Antennas Propag.*, vol. 14, no. 4, pp. 440–450, Jul. 1966.
[24] A. Jenkins, V. Bana, and G. Anderson, "Impedance of a coil in seawater," in *IEEE Antennas Propag. Soc. Int. Symp. (APSURSI)*, Jul. 2014.
[25] M. B. Kraichman, "Impedance of a circular loop antenna in a infnite conducting medium," *J. Res. Nat. Bur. of Std. Radio Propag.*, vol. 66D, no. 4, Jul. 1962.
[26] J. R. Wait, "Insulated loop antenna immersed in a conducting medium," *J. Res. Nat. Bur. of Std.*, vol. 59, no. 2, Aug. 1957.
[27] S. Babic, F. Sirois, C. Akyel, and C. Girardi, "Mutual inductance calculation between circular filaments arbitrarily positioned in space: Alternative to grover's formula," *IEEE Trans. Magn.*, vol. 46, no. 9, pp. 3591–3600, Sep. 2010.
[28] C. Zhang, W. Zhong, X. Liu, and S. Y. R. Hui, "A fast method for generating time-varying magnetic field patterns of mid-range wireless power transfer systems," *IEEE Trans. Power Electrons.*, vol. 30, no. 3, pp. 1513–1520, Mar. 2015.
[29] P. Hadadtehrani, P. Kamalinejad, R. Molavi, and S. Mirabbasi, "On the use of conical helix inductors in wireless power transfer systems," in *IEEE Canadian Conf. Elect. Comp. Eng. (CCECE)*, May 2016.
[30] X. Shi, C. Qi, M. Qu, S. Ye, G. Wang, L. Sun, and Z. Yu, "Effects of coil shapes on wireless power transfer via magnetic resonance coupling," *Journal of Electromagnetic Waves and Applications*, vol. 28, no. 11, pp. 1316–1324, 2014.
[31] Z. Zeng, S. Fu, H. Zhang, Y. Dong, and J. Cheng, "A survey of underwater optical wireless communications," *IEEE Commun. Surveys Tuts.*, vol. 19, no. 1, pp. 204–238, Aug. Firstquarter 2017.
[32] V. Jiwariyavej, T. Imura, and Y. Hori, "Coupling coefficients estimation of wireless power transfer system via magnetic resonance coupling using information from either side of the system," *IEEE J. Emerg. Sel. Topics Power Electron.*, vol. 3, no. 1, pp. 191–200, Mar. 2015.
[33] V. Arikatla, "Adaptive control methods for dc-dc switching power converters," Ph.D. dissertation, Univ. of Alabama, 2011.
[34] J. Tian and A. P. Hui, "A dc-voltage-controlled variable capacitor for stabilizing the zvs frequency of a resonant converter for wireless power transfer," *IEEE Trans. Power Electrons.*, vol. 32, no. 3, pp. 2312–2318, Mar. 2017.

Taofeek Orekan (M'14) received the B.S. degree in electrical engineering from Kennesaw State University, Atlanta, GA, USA, M.S. degree in electrical engineering from University of Connecticut, Storrs, CT, USA, and currently he is a Ph.D. candidate in electrical engineering at University of Connecticut. His research interests include control of wireless power transfer systems, renewable energy, smart ocean systems and smart grid.

Taofeek is a member of CIGRÉ, IEEE Young Professionals, and IEEE-HKN. He was a recipient of the prestigious NSF GK-12 Fellowship award in 2014 and 2015.

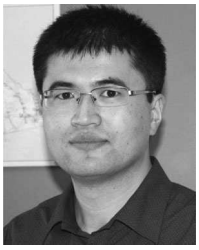

Peng Zhang (M'07−SM'10) received the Ph.D. degree in electrical engineering from the University of British Columbia, Vancouver, BC, Canada, in 2009. He is the Castleman Professor in Engineering Innovation, and Associate Professor of Electrical Engineering at the University of Connecticut, Storrs, USA. He was a System Planning Engineer at BC Hydro and Power Authority, Vancouver. His research interests include software defined smart grid, microgrids, smart and connected communities/cities, cyber security, and smart ocean systems. Dr. Zhang is a Registered Professional Engineer in BC, Canada, and an individual member of CIGRÉ.

Cyuansi Shih is a PhD candidate in Mechanical Engineering from University of Connecticut. He received his M.S. degree in Engineering Science from National Taiwan University. His research is in the area of dynamics and control, adaptive cooperative control and bio-mechanics.